

Electrochemical ferroelectric switching: The origin of polarization reversal in ultrathin films

N. C. Bristowe,^{1,2} Massimiliano Stengel,^{3,4} P. B. Littlewood,^{1,5} J. M. Pruneda,⁶ and Emilio Artacho²

¹Theory of Condensed Matter, Cavendish Laboratory,
University of Cambridge, Cambridge CB3 0HE, UK

²Department of Earth Sciences, University of Cambridge, Downing Street, Cambridge CB2 3EQ, UK

³ICREA - Institutó Catalana de Recerca i Estudis Avançats, 08010 Barcelona, Spain

⁴Institut de Ciència de Materials de Barcelona (ICMAB-CSIC), Campus UAB, 08193 Bellaterra, Spain

⁵Physical Sciences and Engineering, Argonne National Laboratory, Argonne, Illinois 60439, USA

⁶Centre d'Investigació en Nanociència i Nanotecnologia (CSIC-ICN), Campus UAB, 08193 Bellaterra, Spain

(Dated: March 1, 2022)

Against expectations, robust switchable ferroelectricity has been recently observed in ultrathin (1 nm) ferroelectric films exposed to air [V. Garcia *et al.*, Nature (London) **460**, 81 (2009)]. Based on first-principles calculations, we show that the system does not polarize unless charged defects or adsorbates form at the surface. We propose electrochemical processes as the most likely origin of this charge. The ferroelectric polarization of the film adapts to the external ionic charge generated on its surface by redox processes when poling the film. This, in turn, alters the band alignment at the bottom electrode interface, explaining the observed tunneling electroresistance. Our conclusions are supported by energetics calculated for varied electrochemical scenarios.

I. INTRODUCTION

Complex oxides have long been viewed as possible candidates for the next generation of electronic devices, which require reduced feature sizes, enhanced operating speeds and low consumption. Amongst oxides, ferroelectrics offer the ability to store information in a non-volatile manner via fast reversible polarization switching in ferroelectric random-access memory (FeRAM). The observation of giant tunneling electroresistance (TER)¹ in ultrathin (3 unit cells) ferroelectric films has recently opened a novel paradigm for device design based on these materials^{2,3}.

Although the experiments¹ ascribed TER to ferroelectricity, which appeared robust and switchable, how the polar state is stabilized in such thin films is by no means established. In principle, a ferroelectric film with an exposed surface cannot sustain a monodomain polarization perpendicular to the surface, because of the strong depolarizing field that would inevitably arise³⁹. Charged particles from the environment could in principle cancel the depolarizing field⁴ (Fig. 1 left). So far, however, the only chemical control of switching in air relates to neutral species, O₂⁵⁻⁷ (Fig. 1 center). It is then not clear how neutral gas-phase molecules could interact with a biased atomic force microscopy (AFM) tip to produce the polar state.

Here we argue that the voltage applied with the AFM tip induces electrochemical switching (Fig. 1 right), i.e. redox processes that are essential to liberate free charge and therefore screen the depolarizing field. This process would act as a nanobattery, rather than a nanocapacitor. Note that the same mechanism could explain other effects at oxide interfaces, such as the switchable two-dimensional electron gas (2DEG) at the LaAlO₃/SrTiO₃ interface^{8,9}, where the switching appears to be mediated

by surface charge¹⁰.

To explore this mechanism we consider the system studied experimentally in Ref. 1, consisting of a compressively strained nanometer-thick BaTiO₃ (BTO) film on a La_{0.7}Sr_{0.3}MnO₃ (LSMO) bottom electrode. Here we show, using first principles calculations, that (i) the pristine system (clean BTO surface with an ideal TiO₂ termination) does not allow for a ferroelectric polarization, *P*, normal to the surface despite the large compressive strain; (ii) a non-zero *P* is crucially dependent on the presence of a surface external ionic charge, in the form of defects or adsorbates; and (iii) the energetics for the formation of oxidized or reduced surface defects support the electrochemical switching model. We also find (iv) a systematic change in band offset with screening charge density, which we identify as the microscopic mechanism behind the experimentally observed TER¹, and (v) a large magnetoelectric coupling, due to the accumulation or depletion of spin-polarized carriers at the

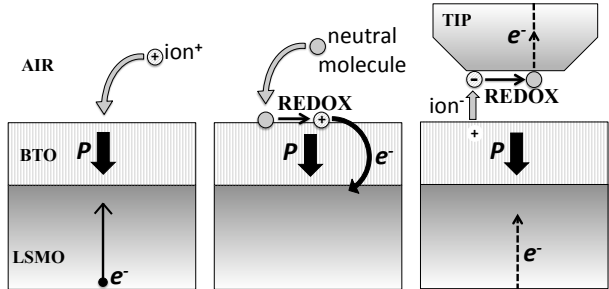


FIG. 1: Schematic illustration of the conventional (left) and redox (center) mechanisms for ferroelectric screening in the absence of a top electrode. The presence of a biased tip can promote an alternative redox mechanism that provides an external circuit for the screening electrons (right).

interface with ferromagnetic LSMO. The connection between these effects can be summarized as follows: under open-circuit boundary conditions the electric displacement field D within the film, the change in magnetization at the interface ΔM and the interface dipole, are all proportional (or equal) to the external ionic charge density, Q per unit surface S , produced by the redox processes.

II. METHODS

The density-functional theory (DFT) calculations are performed using the spin-polarized Wu-Cohen (WC) exchange-correlation functional¹¹, as implemented in the SIESTA code^{12,13,40}. We find GGA-WC to reproduce bulk¹⁴ and surface^{14,15} properties of LSMO that were calculated using the Perdew-Burke-Ernzerhof (PBE) scheme¹⁶; at the same time, GGA-WC is more appropriate for ferroelectric oxides. The LSMO/BTO system consists of 5.5 unit cells of LSMO (MnO₂-terminated) stacked with 3 unit cells of BTO along the c direction in a slab geometry. The supercell contains a 15 Å thick vacuum layer and has either 2×2 or $\sqrt{2} \times \sqrt{2}$ in-plane periodicity (see Fig. 2). The 5.5 unit cells of LSMO are thick enough to show bulk-like features in the center, and 3 unit cells of BTO was experimentally shown to be thick enough for ferroelectricity¹. We use a dipole correction to simulate open-circuit boundary conditions, enforcing zero macroscopic electric field in the vacuum layer. We constrain the in-plane lattice parameter to experimental bulk NdGaO₃ (NGO) to reproduce the experimental conditions of Ref.¹; this imposes a large (3%) compressive strain on BTO. Based on this slab geometry, we perform a number of calculations where we vary the surface composition by introducing defects or adsorbates. In particular, we simulate the clean TiO₂-terminated surface (we shall refer to this structure as “pristine” henceforth); one O vacancy (“O-vac”) or adatom (“O-ads”) per 2×2 surface cell; one H adatom (“H”) or OH group (“OH”) per $\sqrt{2} \times \sqrt{2}$ cell⁴¹. Hereafter we shall discuss the results with special regard for the presence or absence of ferroelectric polarization in each case.

III. DISCUSSION

A. The pristine system

Fig. 2 shows the relaxed out-of-plane structural distortions as a function of the surface chemical environment. The pristine system is characterized by negligible distortions in the interior of the BTO film, suggesting the absence of macroscopic P in this system. Only a surface rumpling is present, resulting in a small net inwards dipole (non-switchable) that decays rapidly towards the bulk (a surface rumpling is a known general feature of oxide surfaces, in particular the TiO₂ termination of BTO^{17,18}). A vanishing P is consistent with the

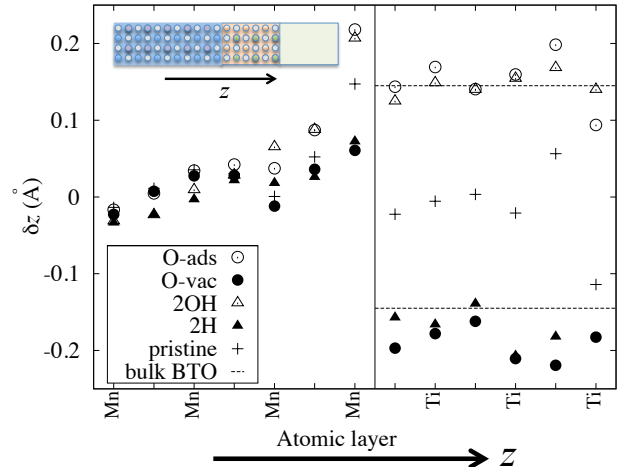


FIG. 2: (Color online) Cation-anion splittings, $\delta z = z_{\text{cation}} - z_{\text{anion}}$ through the LSMO/BTO slab (the bottom half of LSMO is not shown). The dotted lines correspond to the average of the AO and BO₂ layer anion-cation splitting for the inwards and outwards P in bulk BTO, strained to NGO.

open-circuit boundary conditions, despite the large compressive strain. In absence of a top electrode the macroscopic electric displacement field D in BTO is equal and opposite to the density of external surface charge. As this charge is zero at the clean TiO₂ surface, the film is constrained to a paraelectric state.

B. Chemical switching

To illustrate possible screening scenarios, we now include representative surface defects⁴². The O-vac and O-ads systems are both characterized by large ferroelectric distortions (Fig. 2). These are comparable to the strained bulk, where we calculate a spontaneous polarization $P_0 = 0.369 \text{ C/m}^2$ (0.35 e/S). This result is again consistent with the constraint that $D = -Q/S$. In fact, one oxygen defect for every 2×2 unit cells (0.5 e/S) yields a larger surface charge than what would be sufficient to screen P_0 . This justifies the larger cation-anion rumplings that we obtain in the film compared with the bulk (Fig. 2). OH and H adatoms (with $\sqrt{2} \times \sqrt{2}$ coverage to maintain Q/S) produce distortions of similar magnitude (Fig. 2). This confirms the generality of the ferroelectric switching mechanism: the ferroelectric state really depends on the net surface charge, and not on the chemical identity of the adsorbed species.

In order to study the electrochemical switching (Fig. 1 right), we commence by analyzing *chemical* switching (Fig. 1 center). Both are controlled by redox processes that transform bound charge into free charge, allowing for an electronic transfer between the surface defect and the metal substrate, but have different associated chemical sources/drains and energetics. Chemical switching was recently shown in a system consisting of PbTiO₃ on

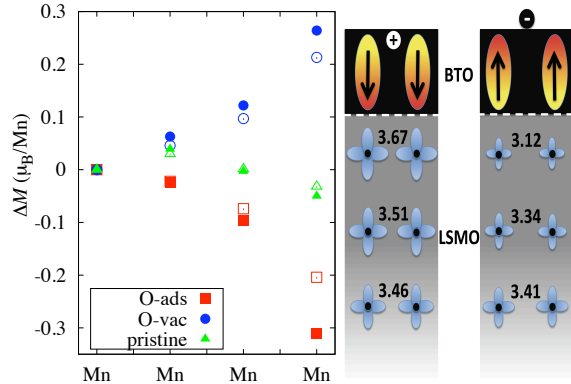


FIG. 3: (Color online) Change in Mn magnetic moment (left), ΔM , near the interface (the interface MnO_2 layer is on the right). Open symbols represent the change in $3d\ e_g$ occupation, and closed symbols the total magnetic moment. A schematic illustration (right) of the effect of O-vac and O-ads on the BTO polarization (arrows) and the Mn $3d\ e_g$ occupation (blue lobes) and total Mn magnetic moment (numbers).

$\text{SrRuO}_3^{5,6}$ and BTO films on Au or vacuum⁷.

To assess whether these redox reactions are thermodynamically accessible in typical experimental conditions, we estimate the formation energy of the defective systems taking the reactions: 1) Slab(pristine) \rightarrow Slab(O-vac)+1/2 O_2 and equivalent for O-ads, 2) 1/2 H_2O +1/4 O_2 +Slab(pristine) \rightarrow Slab(OH) and 3) 1/2 H_2O +Slab(pristine) \rightarrow Slab(H)+1/4 O_2 . The chemical potential of the relevant molecular species is set to the calculated total energy of the spin-polarized molecule in a large cubic box. The results are summarized in Table 1. They suggest that, whilst the oxygen adatom is likely to form under oxygen-rich conditions, the formation energy for the oxygen vacancy is possibly too high to form even in oxygen-poor conditions. The calculated OH and H formation energies suggest that water is a very likely redox intermediate. Note that H_2O is ubiquitous in most experiments performed in air, and was recently found to play a crucial role in AFM experiments performed on $\text{LaAlO}_3/\text{SrTiO}_3^{19}$. Since both sets of reactions involve oxygen, we therefore expect that altering the surrounding oxygen partial pressure would affect the stability of reduction or oxidation processes, consistent with the recently observed chemical switching⁵.

TABLE I: The formation energy, E_f , of the defective systems for O_2 and H_2O rich conditions (see text for definitions).

| | O-vac | O-ads | OH | H |
|------------|-------|-------|------|------|
| E_f (eV) | +3.6 | -0.4 | -1.5 | +0.9 |

C. Electrochemical switching

Now we discuss how the electrochemical processes could proceed in practice during the AFM switching experiments of Ref. 1 (general electrochemical processes on oxide surfaces are reviewed in Ref. 20,21). As schematically shown in Fig. 1 (right), a biased tip close to contact can remove surface ions. These would then undergo a redox reaction at the tip surface. This process is favored by the energy associated with the biased external circuit, QV_{ext} , but costs an energy equal to the change in binding energy of the ion to the ferroelectric surface and to the tip surface, ΔE_f (this effectively redefines the relevant chemical potential). By minimizing the Gibbs free energy of the system (see e.g. Ref. 22 or 23) it can be shown that poling can stabilize redox defects if $V_{ext} > \Delta E_f/Q$, after which the equilibrium redox charge density, Q/S , and polarization both grow with V_{ext} . This electrochemical process would then act as a nanobattery, rather than a nanocapacitor. By controlling the environment (species and chemical potential) and V_{ext} , one may be also able to selectively control the active redox reaction, potentially opening new routes to surface redox catalysis. After removal of the tip, the surface redox density from poling can remain, since the reverse reaction is now blocked by key reactants being removed with the tip. This would explain the observation of Ref. 1 that the domains are stable for a very long time after “writing”. Of course, lateral charge diffusion across domain boundaries²⁴ may still occur in principle, but kinetic barriers are likely to hinder such processes. Therefore the bulk polarization, P_0 , is expected to be an estimate of the equilibrium polarization after poling. We note that unlike in the $\text{LaAlO}_3/\text{SrTiO}_3$ system where the polarization is driving the surface chemistry⁹, in ferroelectric films we expect it is the surface chemistry (and poling) that is driving the polarization. This is because the energy scale for changing the polarization is much larger in LaAlO_3 than in the ferroelectric.

D. Magnetoelectric coupling

The electronic transfer mechanism can be quantitatively estimated through the change in magnetization of LSMO. LSMO is a half-metal with only Mn $3d\ e_g$ majority spin levels around the Fermi level. As the screening carriers are fully spin-polarized, an electronic transfer between LSMO and the BTO surface results in a systematic change of the magnetization near the interface. We calculate the change in magnetization from the pristine to the O-vac and O-ads systems and to the 2OH and 2H systems, ΔM , as $\pm 1.7\ \mu_B$ and $\pm 1.5\ \mu_B$ in the supercell, equivalent to $\pm 0.42\ e/S$ and $\pm 0.37\ e/S$ respectively (the remaining 0.1 electrons/holes stay in BTO, see Appendix). This extra electron density (which corresponds to the electric displacement, D , because of the half-metallic nature of LSMO) resides in the interface

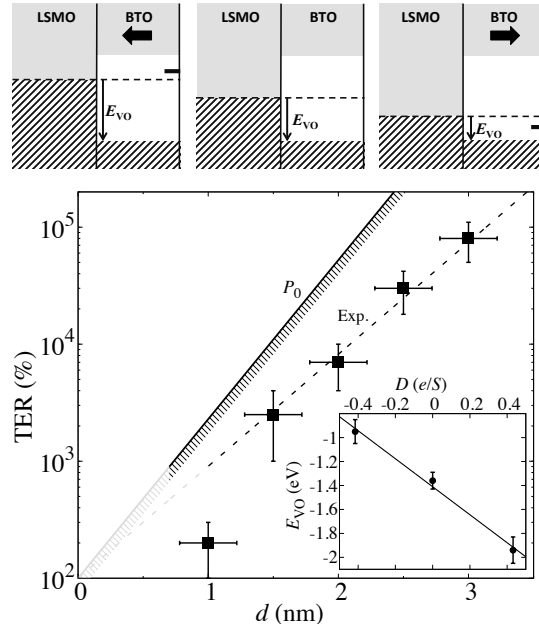


FIG. 4: Top: Schematic illustration of the change in band offset, E_{VO} , with polarization reversal. Bottom: Tunnel electroresistance (TER) vs BTO thickness. Experimental points taken from Garcia *et al.*¹ (squares with dashed line fit) are compared with a theoretical expression²⁵ which uses the tunneling barrier height expected from the BTO bulk polarization, P_0 (solid line). Inset: Calculated band offset against electric displacement field for the three BTO states. The straight line fit is used to determine the band offset (and hence barrier height) at $\pm P_0$ for the TER plot.

region, decaying into the electrode with an associated Thomas-Fermi screening length (see Fig. 3). This situation is similar to the carrier-mediated magnetoelectricity already predicted at SrTiO₃/SrRuO₃ interfaces²⁶ and in LSMO/BTO superlattices²⁷. In agreement with Ref. 27 a competing interface antiferromagnetic type phase (called A₁ in Table 1 of Ref. 27) was found for the outwards BTO polarization. A similar magnetoelectric effect has recently been experimentally realized^{28,29}.

E. Tunneling Electroresistance

We now discuss how the electrochemical switching process may lead to the giant TER observed in the LSMO/BTO system¹. In the simplest semiclassical approximation, TER has an exponential dependence on the tunneling barrier shape²⁵. The interface dipole, and hence band offset ($E_{VO} = E_{VBm} - E_F$), at a metal/ferroelectric interface depends linearly on the electric displacement field, D , in a way that can be expressed with an effective screening length^{30–32}, λ_{eff} . For LSMO-BTO we calculate $\lambda_{eff} = 0.11$ Å. Using the calculated values of the band offset (Fig. 4 inset) and the experimental band gap of BTO, we obtain the change in barrier

height upon complete polarization reversal (for $D = \pm P_0$ the potential in BTO is flat, i.e. the tunneling barrier shape is rectangular), $\Delta\varphi$, and the average barrier height, $\bar{\varphi} = (\varphi_{out} + \varphi_{in})/2$. These values then yield an estimate of the TER using the exponential dependence²⁵ on the barrier thickness, d , for large TER,

$$\text{TER} \approx \exp \left[\frac{\sqrt{2m}}{\hbar} \frac{\Delta\varphi}{\sqrt{\bar{\varphi}}} d \right]. \quad (1)$$

Fig. 4 compares this estimate with the experimental data¹ showing that this simple model captures remarkably well the essential physics of TER in this system. We note a recent study reported comparable shifts in E_{VO} (measured using photoelectron spectroscopy) on a similar ferroelectric/LSMO system upon polarization reversal³³. The origin of electroresistance effects in oxide nanotubes has also recently been suggested as redox reactions³⁴. However the redox arguments there are fundamentally different – it is proposed that the electrons yielded by oxygen vacancies are directly available for conduction.

IV. CONCLUSIONS

In conclusion we have studied an electrochemical mechanism for ferroelectric switching in thin films and proposed it as the origin of switchable ferroelectricity, TER and magnetoelectricity in a prototypical system. This work opens several avenues for future research. From the experimental point of view, it would be interesting to investigate the composition of a ferroelectric surface before and after switching (e.g. via the AFM tip), to verify whether reduced or oxidized gas-phase species are present (as suggested by our results). Also, this point could be indirectly checked by performing the AFM-mediated switching experiments in a controlled atmosphere, in analogy to the experiments of Bi *et al.* [19] on LAO/STO. From the theoretical point of view, a natural next step would be to perform a more detailed thermodynamic analysis of the stability of a ferroelectric surface (either pristine or decorated with adsorbates). This would involve exploring different coverages, possible inhomogeneous polarization states, and the effect of temperature and other external perturbations. We hope that our results will stimulate further investigations along these (and possibly other) directions.

Acknowledgments

We acknowledge G Catalan, J Íñiguez, M Bibes, V Garcia, N Mathur, X Moya, J Junquera, C Ocal and S Streiffer for valuable discussions, the support of EP-SRC, NANOSELECT and MCINN FIS2009-12721-C04-01 and computing resources of CamGRID at Cambridge, the Spanish Supercomputer Network and HPC Europa. PBL acknowledges DOE support under FWP 70069.

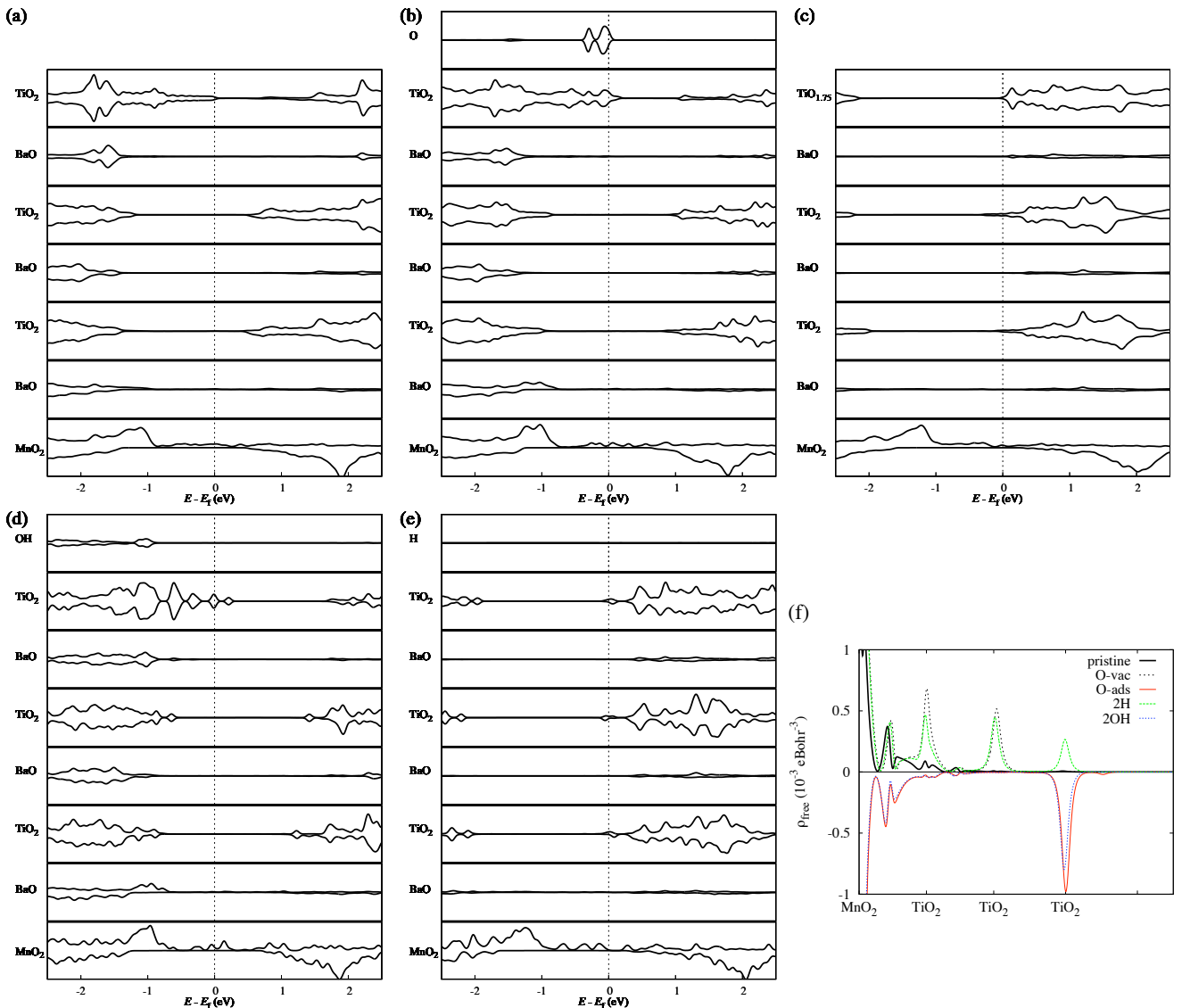


FIG. 5: (Color online) Spin-resolved layer-by-layer density of states centered around E_f for the LSMO/BTO systems. Positive DOS represents majority spin, negative DOS minority spin. Only the BTO layers (and 1 LSMO layer) are shown for clarity. Panels (a)-(e) correspond to pristine, O-ads, O-vac, 2OH and 2H systems respectively. Panel (f) shows a profile of ρ_{free} through the various LSMO/BTO systems.

Appendix

Here we provide details of the electronic structure of the various LSMO/BTO systems. Figure 5 (a)-(e) shows the spin-resolved layer-by-layer density of states for the pristine, O-ads, O-vac, 2OH and 2H systems. As discussed in the main text, the electric displacement and polarization within BTO, D and P , and hence the valence band offset, E_{VO} , depend only on Q/S , the surface defect charge density, and not the surface chemistry. However, as discussed in Ref. 35, this is not strictly the case once E_{VO} becomes negative or reaches the band gap of BTO. At this point electrons or holes “spill out” in to the BTO layer. This “charge spill out” regime is favored by DFT, which often underestimates the band gap, and

therefore can be an artifact of the calculation.

In our case, due to the presence of a free surface, there is a further issue that was not explicitly considered in Ref. 35, i.e. the effect of surface states. In many cases, these fall within the bulk band gap of the ferroelectric film, and might cross the Fermi level of the metal, thus causing a significant spill-out of charge even when the bulk electronic bands are not directly affected. Note that surface states in ferroelectrics typically have a marked localized orbital character (either the atomic orbital of an adsorbate, or the $3d$ orbitals of the transition metal cation). Therefore, it is reasonable to suspect that DFT might introduce systematic errors in their ionization energies (similarly to the energy location of the bulk band edges discussed in Ref. 35), and the metallization of a

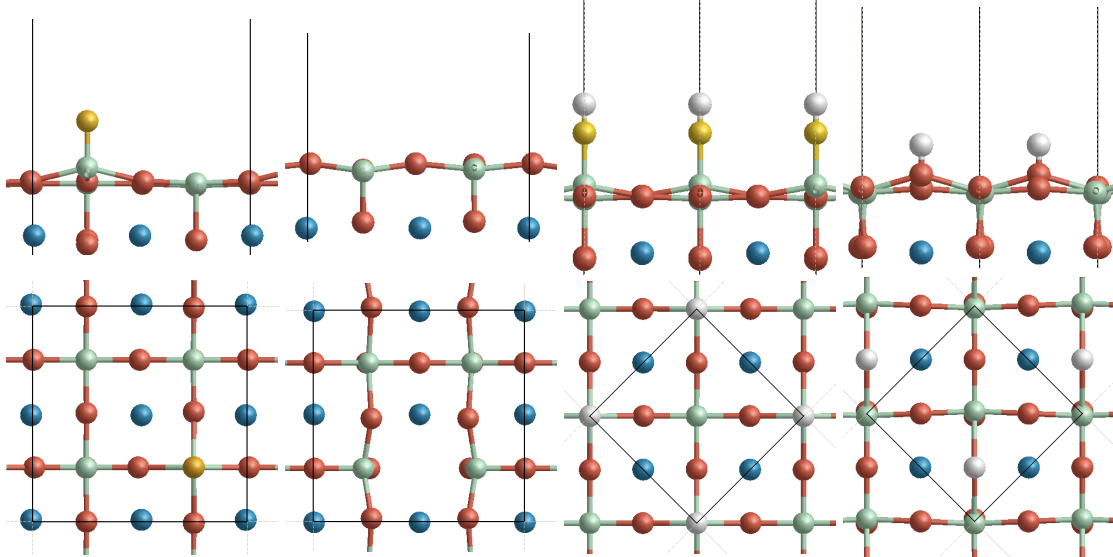


FIG. 6: Relaxed surface LSMO/BTO structure. Top: view along the [100] direction. Bottom: birds-eye view along the [001] direction. Only the top BTO layer is shown for clarity. Sr (blue), Ti (cyan), O (red), O-ads (orange). Panels correspond to O-ads, O-vac, 2OH and 2H systems respectively (left to right).

surface state should be regarded with analogous caution (for a detailed discussion of charge transfers at surfaces see, e.g., Ref. 36).

Refs. 35 and 36 prescribe an analysis of the hole- and electron-like charge spill out. Following this prescription, we determine the free electron density profile, ρ_{free} , within BTO in Fig. 5(f) (using Eq. 25 and 26 of Ref. 35 and Eq. 19 of Ref. 36 for hole spill out). Out of all the five systems, the pristine one is unaffected, the negatively polarized (O-vac and 2H) systems are affected by electron spill out into the conduction band, and the two positively polarized (O-ads and 2OH) ones are affected by hole spill out into surface states (see Fig. 5). In both O-vac and 2H ρ_{free} amounts to approximately 0.03 electrons per unit cell of BTO, which is a fairly mild effect (compare with approximately 0.15 electrons per unit cell in the KNO/SRO system of Ref. 35). In the case of O-ads and 2OH, the surface O(2p) states accommodate a total of approximately 0.1 holes per surface perovskite unit (Fig. 5(f)). Of course, estimating to what degree this charge spill is problematic, depends not only on the magnitude but also the purpose of the calculation. The charge spill out induces an error in two quantities that are discussed in this work: the total injected charge into the LSMO electrode, and the band alignment. Consider-

ing the total injected charge, the impact of this error is trivial to estimate. In fact, 0.03 electrons per cell times N , number of BTO cells, corresponds exactly to the difference between the actual induced spin in LSMO and the “ideal” limit of 2 Bohr magnetons per cell. This observation can be directly used to estimate the error in the calculated band offset. In fact, we can assume in a first approximation that the band offset is linear in the electric displacement of the BTO cell adjacent to the interface, D_{inter} . Using the above numbers for the O-vac system,

$$D_{inter} = 2e/S - 0.03e(N/S) = M/S = 1.7e/S, \quad (A.1)$$

where M is the induced spin, and S is the supercell surface area (or reciprocal of the defect density). This provides an accurate estimate of the actual electric displacement “felt” by LSMO. Using this information, therefore, we can make a very accurate estimation of the linear band offset dependence with D . We used this analysis to make the plot shown in Fig. 4 inset of the main text. Therefore, whilst we understand the limitations of DFT, in this case they do not affect significantly our conclusions.

Figure 6 displays the relaxed atomic structures of the BTO surface with O-ads, O-vac, 2OH and 2H.

¹ V. Garcia, S. Fusil, K. Bouzehouane, S. Enouz-Vedrenne, N. Mathur, A. Barthélémy, and M. Bibes, *Nature* **460**, 81 (2009).

² P. Zubko and J. Triscone, *Nature* **460**, 45 (2009).

³ M. Segal, *Nature Nanotechnology* (2009).

⁴ V. Fridkin, *Ferroelectric semiconductors* (Consultants Bu-

reau, 1980), ISBN 0306109573.

⁵ R. Wang, D. Fong, F. Jiang, M. Highland, P. Fuoss, C. Thompson, A. Kolpak, J. Eastman, S. Streiffer, A. Rappe, et al., *Phys. Rev. Lett.* **102**, 47601 (2009).

⁶ D. Fong, A. Kolpak, J. Eastman, S. Streiffer, P. Fuoss, G. Stephenson, C. Thompson, D. Kim, K. Choi, C. Eom,

- et al., Phys. Rev. Lett. **96**, 127601 (2006).
- ⁷ J. Spanier, A. Kolpak, J. Urban, I. Grinberg, L. Ouyang, W. Yun, A. Rappe, and H. Park, Nano Lett. **6**, 735 (2006).
 - ⁸ C. Cen, S. Thiel, G. Hammerl, C. W. Schneider, K. E. Andersen, C. S. Hellberg, J. Mannhart, and J. Levy, Nat. Mater. **7**, 298 (2008).
 - ⁹ N. C. Bristowe, P. B. Littlewood, and E. Artacho, Phys. Rev. B **83**, 205405 (2011).
 - ¹⁰ Y. Xie, C. Bell, T. Yajima, Y. Hikita, and H. Hwang, Nano Lett. (2010).
 - ¹¹ Z. Wu and R. Cohen, Phys. Rev. B **73**, 235116 (2006).
 - ¹² P. Ordejon, E. Artacho, and J. M. Soler, Phys. Rev. B **53**, 10441 (1996).
 - ¹³ J. Soler, E. Artacho, J. Gale, A. Garcia, J. Junquera, P. Ordejon, and D. Sanchez-Portal, J. Phys.: Condens. Matter **14**, 2745 (2002).
 - ¹⁴ V. Ferrari, J. Pruneda, and E. Artacho, Physica Status Solidi (a) **203**, 1437 (2006).
 - ¹⁵ J. Pruneda, V. Ferrari, R. Rurali, P. Littlewood, N. Spaldin, and E. Artacho, Phys. Rev. Lett. **99**, 226101 (2007).
 - ¹⁶ J. Perdew, K. Burke, and M. Ernzerhof, Phys. Rev. Lett. **77**, 3865 (1996).
 - ¹⁷ J. Padilla and D. Vanderbilt, Phys. Rev. B **56**, 1625 (1997).
 - ¹⁸ E. Heifets, S. Dorfman, D. Fuks, and E. Kotomin, Thin Solid Films **296**, 76 (1997).
 - ¹⁹ F. Bi, D. Bogorin, C. Cen, C. Bark, J. Park, C. Eom, and J. Levy, Appl. Phys. Lett. **97**, 173110 (2010).
 - ²⁰ S. Kalinin, S. Jesse, A. Tselev, A. Baddorf, and N. Balke, ACS nano **5**, 5683 (2011).
 - ²¹ R. Waser, R. Dittmann, G. Staikov, and K. Szot, Advanced Materials **21**, 2632 (2009).
 - ²² G. B. Stephenson and M. J. Highland, Phys. Rev. B **84**, 064107 (2011).
 - ²³ A. Morozovska, E. Eliseev, S. Svechnikov, A. Krutov, V. Shur, A. Borisevich, P. Maksymovych, and S. Kalinin, Phys. Rev. B **81**, 205308 (2010).
 - ²⁴ S. Kalinin and D. Bonnell, Nano Lett. **4**, 555 (2004).
 - ²⁵ A. Gruverman, D. Wu, H. Lu, Y. Wang, H. Jang, C. Folkman, M. Zhuravlev, D. Felker, M. Rzchowski, C. Eom, et al., Nano Lett. **9**, 3539 (2009).
 - ²⁶ J. Rondinelli, M. Stengel, and N. Spaldin, Nature Nanotechnology **3**, 46 (2007).
 - ²⁷ J. D. Burton and E. Y. Tsymbal, Phys. Rev. B **80**, 174406 (2009).
 - ²⁸ C. A. F. Vaz, J. Hoffman, Y. Segal, J. W. Reiner, R. D. Grober, Z. Zhang, C. H. Ahn, and F. J. Walker, Phys. Rev. Lett. **104**, 127202 (2010).
 - ²⁹ H. Molegraaf, J. Hoffman, C. Vaz, S. Gariglio, D. van der Marel, C. Ahn, and J. Triscone, Advanced Materials **21**, 3470 (2009).
 - ³⁰ J. Junquera and P. Ghosez, Nature **422**, 506 (2003).
 - ³¹ M. Zhuravlev, R. Sabirianov, S. Jaswal, and E. Tsymbal, Phys. Rev. Lett. **94**, 246802 (2005).
 - ³² H. Kohlstedt, N. Pertsev, J. Rodríguez Contreras, and R. Waser, Phys. Rev. B **72**, 125341 (2005).
 - ³³ C.-L. Wu, P.-W. Lee, Y.-C. Chen, L.-Y. Chang, C.-H. Chen, C.-W. Liang, P. Yu, Q. He, R. Ramesh, and Y.-H. Chu, Phys. Rev. B **83**, 020103 (2011).
 - ³⁴ S. Nonnenmann, E. Gallo, and J. Spanier, Appl. Phys. Lett. **97**, 102904 (2010).
 - ³⁵ M. Stengel, P. Aguado-Puente, N. A. Spaldin, and J. Junquera, Phys. Rev. B **83**, 235112 (2011).
 - ³⁶ M. Stengel, Phys. Rev. B **84**, 205432 (2011).
 - ³⁷ D. Schlom, L. Chen, C. Eom, K. Rabe, S. Streiffer, and J. Triscone, Annu. Rev. Mater. Res. **37**, 589 (2007).
 - ³⁸ J. Junquera, M. Zimmer, P. Ordejon, and P. Ghosez, Phys. Rev. B **67** (2003).
 - ³⁹ The polarization is clearly observed to be perpendicular to the interface, consistent with the expected behavior of compressively strained films³⁷.
 - ⁴⁰ Details of the pseudopotentials, numerical atomic orbitals and LSMO doping are given in Ref. 14 and 38.
 - ⁴¹ Atomic forces were relaxed to less than 40 meV/Å.
 - ⁴² Sampling the entire phase space (redox species and density, temperature, partial pressure, polarization) is beyond the scope of this work, but can be done within thermodynamic theory (see Ref. 22).